Ceramics International

Cerium-doped gadolinium-scandium-aluminum garnet powders: synthesis and use in X-ray luminescent diamond composites

--Manuscript Draft--

Manuscript Number:	CERI-D-21-10611R1
Article Type:	Full length article
Keywords:	GSAG:Ce, garnets, solid solution, ceramic powder, diamond composite, CVD
Corresponding Author:	Sergey Viktorovich Kuznetsov, Ph.D. A.M. Prokhorov General Physics Institute Russian Academy of Sciences Moscow, RUSSIAN FEDERATION
First Author:	Sergey Viktorovich Kuznetsov, Ph.D.
Order of Authors:	Sergey Viktorovich Kuznetsov, Ph.D.
	Vadim S. Sedov, Dr.
	Artem Martyanov, Dr.
	Sergey Batygov, Dr.
	Dmitrii Vakalov, Dr.
	Kirill Boldyrev, Dr.
	Ivan Tiazhelov
	Soumen Mandal, Dr.
	Henry Bland, Dr.
	Oliver Williams, Prof.
	Marina Nikova, Dr.
	Vitalii Tarala, Dr.
	Alexey Popovich
	Dmitrii Pasternak
Abstract:	Powders of single-phase solid solutions based on cerium-doped gadolinium-scandium-aluminum garnet were synthesized by coprecipitation from aqueous solutions followed by annealing at 1600 °C. The solubility limit of cerium in gadolinium-scandium-aluminum garnet was determined by X-ray powder diffraction and scanning electron microscopy. It has been demonstrated that the solubility limit of cerium depends not only on the concentration of scandium in the solid solution but also on the fraction of Sc^{3+} cations in the dodecahedral and octahedral positions of the garnet crystal lattice. Based on the X-ray luminescence spectra of Ce^{3+} (~575 nm, 5d-4f transition) in single-phase samples, the composition $(Gd_{2.73}Ce_{0.02}Sc_{0.5}Al_{4.75}O_{12})$ with the highest X-ray luminescence was determined. A diamond composite “Diamond-GSAG:Ce” with $Gd_{2.73}Ce_{0.02}Sc_{0.5}Al_{4.75}O_{12}$ particles has been fabricated, which exhibits intense yellow X-ray luminescence, that is visible to the eye. The investigated class of composites is promising for applications in stable detectors and visualizers of high-intensity X-ray radiation in synchrotrons and free-electron lasers.

Cerium-doped gadolinium-scandium-aluminum garnet powders: synthesis and use in X-ray luminescent diamond composites

S.V. Kuznetsov[a], V.S. Sedov[a], A.K. Martyanov[a], S.Ch. Batygov[a], D.S. Vakalov[b], K.N. Boldyrev[c], I.A. Tiazhelov[a], H. Bland[d], S. Mandal[d], O. Williams[d], M.S. Nikova[b], V.A. Tarala[b]

[a]Prokhorov General Physics Institute of the Russian Academy of Sciences, Moscow, 119991, Russia
[b]North Caucasus Federal University, 355009, Stavropol, Russia
[c]Institute of Spectroscopy of the Russian Academy of Sciences, Troitsk, Moscow, 108840, Russia
[d]School of Physics and Astronomy, Cardiff University, CF24 3AA Cardiff; UK

kouznetzovsv@gmail.com

Abstract

Powders of single-phase solid solutions based on cerium-doped gadolinium-scandium-aluminum garnet were synthesized by coprecipitation from aqueous solutions followed by annealing at 1600 °C. The solubility limit of cerium in gadolinium-scandium-aluminum garnet was determined by X-ray powder diffraction and scanning electron microscopy. It has been demonstrated that the solubility limit of cerium depends not only on the concentration of scandium in the solid solution but also on the fraction of Sc^{3+} cations in the dodecahedral and octahedral positions of the garnet crystal lattice. Based on the X-ray luminescence spectra of Ce^{3+} (~575 nm, 5d→4f transition) in single-phase samples, the composition ($Gd_{2.73}Ce_{0.02}Sc_{0.5}Al_{4.75}O_{12}$) with the highest X-ray luminescence was determined. A diamond composite "Diamond-GSAG:Ce" with $Gd_{2.73}Ce_{0.02}Sc_{0.5}Al_{4.75}O_{12}$ particles has been fabricated, which exhibits intense yellow X-ray luminescence, that is visible to the eye. The investigated class of composites is promising for applications in stable detectors and visualizers of high-intensity X-ray radiation in synchrotrons and free-electron lasers.

Keywords

GSAG:Ce, garnets, solid solution, ceramic powder, diamond composite, CVD.

Introduction

In the past few years, a new class of optically active diamond-based composite materials has been proposed and developed. It is based on the introduction of luminescent rare-earth micro- and nanoparticles into a transparent diamond matrix. Such diamond composites with Eu(III) tri-(2,6-pyridine dicarboxylic acid [1], EuF_3 [2], HoF_3 [3], CeF_3 [4], β-$NaGdF_4$:Eu [5], YSAG:Ce and YAG:Ce [6,7] already have shown intense electro-, photo- and X-ray luminescence (XRL).

The developed composites are promising for use as electroluminescent films [3,4], visualizers and scintillators of high-intensity X-ray radiation in free-electron lasers (XFELs) and synchrotrons [7,8]. For efficient use in high-power XFEL-type devices, nanosecond decay time and luminescence in the visible range are highly desirable, which was achieved in our previous works on the basis of diamond-based composites with cerium-doped yttrium-aluminum (YAG:Ce) and yttrium-scandium-aluminum garnets (YSAG:Ce) [6,7]. In a previous study[6] by the authors, for both YAG:Ce and YSAG:Ce, the concentration-temperature limits of the existence of single-phase solid solutions were determined. The composition $[Y_{2.98}Ce_{0.02}]\{Al_2\}Al_3O_{12}$, showed the highest XRL intensity among all tested samples. Devys et al [9] showed that it is possible to increase the luminescence light yield by changing the matrix of yttrium-aluminum garnet (YAG) to gadolinium-scandium-aluminum garnet (GSAG), but no detailed investigation of the distribution of cations over crystallographic positions and the

possible elemental ratios for single-phase solid solutions were performed. Kling et al [10] tested $Gd_{2.97}Ce_{0.03}Sc_2Al_3O_{12}$ single crystal as a scintillator for detecting alpha-, beta-, gamma- and neutron radiation, but the chemical composition of the single crystal was not determined. Liu et al in their review [11] summarized that gadolinium-based garnets have higher scintillation light yield than commercially available and widely used $Bi_4Ge_3O_{12}$ (BGO) single crystals.

It is known that gadolinium-aluminum garnets are unstable in their pure form and are not fully formed at low temperatures (≤ 1300 °C). Additionally, at higher temperatures they tend to decompose (≥ 1300°C, $Gd_3Al_5O_{12}$=>$GdAlO_3$+ Al_2O_3) [13]. Two methods of stabilization may be used to avoid these problems. The first method is based on expanding the octahedral and tetrahedral garnet sites replacing aluminum with cations with a larger ionic radius. The most common approach is the complete or partial substitution of aluminum by gallium ($Gd_3Al_{5-x}Ga_xO_{12}$ [14,15]) with larger ionic radius ($r^{VI}(Al^{3+})$ = 0.535 Å; $r^{IV}(Al^{3+})$ = 0.39 Å; $r^{VI}(Ga^{3+})$ =0.62 Å; $r^{IV}(Ga^{3+})$ = 0.47Å [16]). Moreover, in this case, the substitution begins from the tetrahedral garnet site: $Gd_3Al_2Al_3O_{12}$ =>$Gd_3Al_2Ga_3O_{12}$ =>$Gd_3Ga_2Ga_3O_{12}$. The alternative method involves a decrease in the ionic radius of the dodecahedral site by partial replacement of gadolinium ($r^{VIII}(Gd^{3+})$ = 1.053Å [16]) by ions with a smaller ionic radii, e.g., lutetium ($r^{VIII}(Lu^{3+})$ = 0.977Å [16]), while keeping the octahedral and tetrahedral sites unchanged [14,17–19]. At the same time, scandium can replace both dodecahedral and octahedral sites of the garnet lattice in significant amounts [20], which makes it possible to implement both approaches simultaneously and decrease the size of the dodecahedral site. It should be noted that the effective ionic radii in the dodecahedral and octahedral garnet sites differs more strongly from the ionic radii of the target substituted cations than in the considered examples ($r^{VIII}(Sc^{3+})$ = 0.87Å;$r^{VI}(Sc^{3+})$ = 0.735Å [16]).

However, present experimental data on scandium-containing solid solutions with a garnet structure [20–25] are not sufficient to assess the conditions for the stable compositions based on GSAG with different concentrations of scandium in the dodecahedral and octahedral positions. In addition, questions remain about the effect of Sc^{3+} in each of the positions of the garnet crystal lattice on the solubility limits of various alloying components, including cerium in gadolinium-scandium-aluminum garnet (GSAG:Ce).

Thus, the purpose of this work was to study the possible compositions of stable solid solutions based on cerium-doped gadolinium-scandium-aluminum garnets, as well as to determine the compositions with the highest XRL intensity. Furthermore, the optimal composition was used for the formation of the “Diamond-GSAG:Ce” material in order to study its structure, photo- and X-ray luminescence.

Experimental

The following precursors were used for the synthesis of the powders: aqueous ammonia (25%, high purity, SigmaTek), cerium nitrate hexahydrate (analytical grade, JSC Vekton), gadolinium chloride hexahydrate (99.99% LLC Lanhit), aluminum nitrate nonahydrate (98%, Acros Organics), scandium chloride hexahydrate (99.9%, Rare Metals Plant LLC), ammonium sulfate (99%, Stavreakhim LLC) and ethyl alcohol (95%, Ferein). Deionized water (18 MOhm) was used for all operations.

A set of GSAG:Ce compositions (labeled here as **GD_x**, see details in Table 1) with different content of scandium and cerium were selected for synthesis in order to obtain desirable single-phase samples. **GD_1 – GD_5** samples had 0.5 f.u. of scandium in the crystal structure (0.25 f.u. in dodecahedral position) and cerium content from 0.01 to 0.16 f.u. **GD_6 – GD_9** samples had 1.0 f.u. of scandium in the crystal structure (0.25 f.u. in dodecahedral position) and cerium content from 0.01 to 0.16 f.u. **GD_{10} – GD_{15}** samples had 2.0 f.u. of scandium (0.25 f.u. in dodecahedral position) and cerium content from 0.01 to 0.16 f.u. **GD_{16} – GD_{20}** samples had total scandium content of 0.5 f.u. (0.1 f.u. in dodecahedral positions) and cerium concentration from 0.01 to 0.16 f.u. **GD_{21} – GD_{24}** samples had scandium concentration of 1.0 f.u. (0.2-0.8 f.u. in dodecahedral positions) and a cerium concentration of 0.02 f.u. **GD_{25}** sample was prepared without any scandium in composition and with 0.02 f.u. of cerium content.

Precursor powders for GD_1 – GD_{20} compositions were synthesized at room temperature by dropwise addition of a dilute aqueous salt solution into dilute precipitate (ammonia water, 1.59x excess, $C(NH_3)$ = 0.6 mol/l) [21]. The precipitator also includes ammonium sulfate (0.08

M) as a dispersing agent. The volume ratio of the precipitant to salts was 2:1. The precipitation process was assisted by the constant stirring of the reaction mixture. The precipitate was separated (centrifuge TsLU-6-3, PJSC "TNPP") and was washed with a 0.045M aqueous solution of ammonium sulfate. The synthesized precursor powder was dried at 60 °C in an oven.

The spray method was used [22] to synthesize $GD_{21} – GD_{25}$ powders. The set of the main precursors were similar to the previous dropwise synthesis method. However, in the case of spraying, a combination of the concentrated hot salt solution and the concentrated cooled precipitant solution was used. Ammonium sulfate was added to the precipitant (0.45 M) and washing was carried out with an aqueous solution of ammonium sulfate (0.045 M) by vacuum filtration on a funnel.

After drying, all precursor powders were ball-milled in a Pulverisette 5 planetary mill (Fritsch, Germany) with zirconia balls for 30 minutes. An ammonium sulfate aqueous solution was used as a milling medium in GD_1 - GD_{20} samples, and ethyl alcohol was used in $GD_{21} – GD_{25}$ samples. After drying the suspension, the powders were annealed in a high-temperature furnace Nabertherm 40/17 (Germany) at 1600 °C in air. After annealing, the ceramic powders were ground in a mortar.

Empyrean X-ray diffractometer (PANalytical, Netherlands) with CuKα radiation at a wavelength of 1.5406 Å was used to investigate the samples' phase composition and unit cell parameters. The following packages were used for X-ray diffraction analysis: WinXRD v 2.1-1 and HighScorePlus v 3.05 with the ICDDPDF-2 release 2013 database.

The morphology and elemental composition of the samples were studied using a TESCAN MIRA3 scanning electron microscope equipped with the system for determining the elemental composition. (AZtec Energy Standard/X-max 20 (standard) (Tescan, Czech Republic)).

The chemical vapor deposition (CVD) of all polycrystalline diamond films were done in two steps. First, a 6 μm-thick polycrystalline diamond film was grown on silicon (100). This layers was used as a substrate for applying the GSAG:Ce suspension. The second step was the growth of 2 μm diamond layer to encapsulate the GSAG nanoparticles. The diamond growth was performed in hydrogen-methane gas mixtures in a microwave plasma reactor ARDIS-100 (2.45 GHz, Optosystems LLC, Russia) [26]. Growth conditions were as follows: total gas flow was 500 sccm; methane content of 3% CH_4/H_2; pressure of 80 Torr, microwave power of 5 kW, and standard deposition rate of 1 μm per hour. The substrate temperature was maintained at 800 ± 20 ◦C, as measured by a two-color Micron M770 pyrometer, to protect the of GSAG nanoparticles from atomic hydrogen during second growth step. A required number of drops (1÷4, 0.02 ml each) of the suspensions of GSAG:Ce in DMSO with nanodiamond particles (average size 5 nm [27,28]) were applied one-by-one on the first diamond layer. Each droplet was dried separately using SPS SPIN 150 spin coater (3000 rpm, 5 min). The combination of GSAG:Ce and nanodiamond particles facilitates the formation of a thin diamond film on GSAG:Ce in the early stages of the second CVD process, which gives them additional protection from etching by atomic hydrogen. The 2 μm of diamond layer in the second CVD step encapsulates the applied nanoparticles to form a "Diamond-GSAG:Ce" composite.

Photoluminescence (PL) spectra of composite films were taken at room temperature with a LabRam HR840 (Horiba Jobin-Yvon) spectrometer in a confocal configuration. The laser beam at 473 nm wavelength was focused in ≈1 μm spot on the sample surface. A brief scan of the surface was performed before taking high-resolution spectra from the areas with intense Ce^{3+} signal and areas of the regular PCD film far from integrated GSAG particles.

X-ray luminescence spectra (XRL) of pristine GSAG:Ce powders, diamond composite films and membranes were measured by two different laboratory-built installations. The first “closed-chamber”-type setup uses tungsten anode the X-ray source. The sample was placed onto the holder horizontally under the beam of the X-ray source, operating at a voltage of 40 kV and a current of 35 mA. The XRL in the 200–1050 nm region was collected by a waveguide and transferred to an FSD-10 spectrometer (Optofiber LLC, Moscow, Russia). The time of signal registration for powders and diamond-powder composites were 0.5s and 50 s, respectively. The second XRL setup uses copper anode to get lower energies of X-ray radiation and thus allowing an “open-chamber” design. The sample was placed on the holder horizontally under the beam of

the X-ray source, operating at a voltage of 30 kV and a current of 50 mA. The XRL signal in the 200–800 nm spectral region was collected using optical fiber with quartz collimator lens and transferred to an OceanInsight spectrometer model HDX-UV-VIS with 10 μm slit (spectral resolution up to 0.35 nm). The time of signal registration for composite membranes was 10 s.

Results and discussion

The compositions of the samples and the results of their X-ray phase analysis are presented in Table 1. Initially, three groups of GSAG:Ce samples were selected for the study with total scandium content of 0.5 formula units (f.u.), labeled GD_1 – GD_5 (see details in Table 1), 1.0 f.u. (GD_6 – GD_9) and 2.0 f.u. (GD_{10} – GD_{15}), respectively, and the cerium concentration was consistently changed from 0.01 to 0.16 f.u. The proportion of scandium in the dodecahedral position of the garnet remained constant at 0.25 f.u. Diffraction patterns of the samples are shown in Figure 1.

At low scandium concentrations, the samples with a cerium content of 0.08 and 0.16 f.u. showed the presence of impurity phases with a perovskite structure. On increasing the total scandium concentration to 1.0 f.u. the composition was unstable for maximum cerium concentration (0.16 f.u.). An increase in the scandium content to 2.0 f.u. lead to formation of stable compositions for all investigated cerium concentrations. Thus, the scandium content increase in the octahedral garnet site promotes an increase in the maximum dopant concentration, as was previously shown by Devys et al. [9]. However, the collected data leads to the suggestion that the presence of scandium in the octahedral position is not the main and only condition for increasing the solubility of cerium in the crystal lattice of the GSAG solid solution. This point is confirmed by the observation that in the series of samples GD_{16} - GD_{20}, mechanical mixtures were formed at all concentrations of cerium (Table 1, Figures 1 and 2). In this case, the proportion of the impurity phase (perovskite) increased with an increase in the concentration of cerium, which is expected, since Ce^{3+} is not a garnet-forming cation. At the same time, in the GD_1 - GD_5 samples with a scandium concentration (0.5 f.u.), but with a greater fraction of it in the dodecahedral position, the mechanical mixtures were registered only at cerium concentrations of ≥0.08 f.u. This effect indicates that it is possible to stabilize GSAG:Ce solid solutions only at certain ratios of Sc^{3+} concentrations in the dodecahedral and octahedral positions of the crystal lattice of the facet.

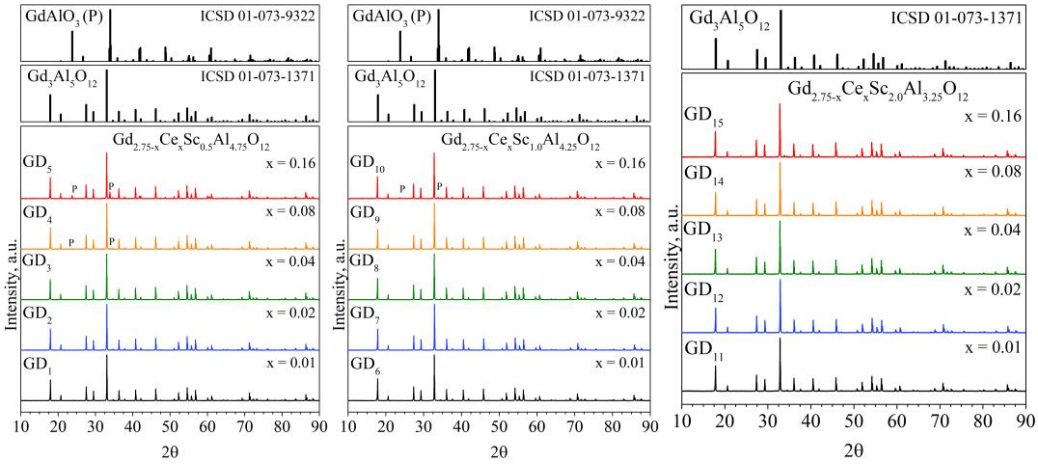

Fig. 1. XRD diffraction patterns of GD_1 – GD_{15} powders annealed at 1600 °C

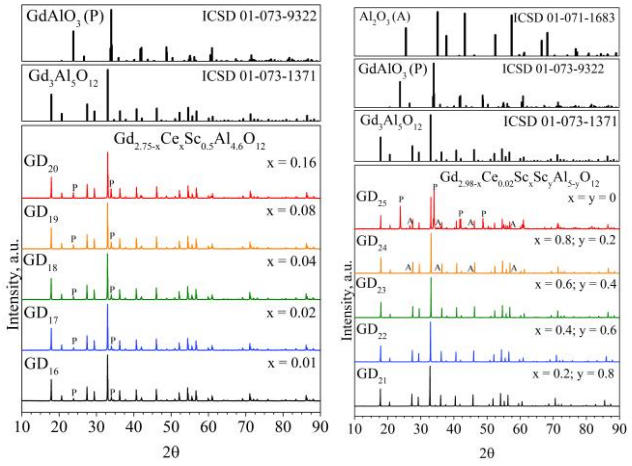

Fig. 2. XRD diffraction patterns of GD_{16} – GD_{25} powders annealed at 1600 °C

Table 1. Composition and characteristics of the synthesized oxide compositions

Sample	Number in Fig.3	XRL intensity, arb. unit	Nominal composition	Ce, f.u.	Sc, f.u.	r^{VIII}, Å	r^{VI}, Å	r^{IV}, Å	r^{IV}/r^{VIII}	Tolerance factor τ [23]	XRD data						
											G, wt.%	a, Å	$GdAlO_3$, %	a, Å	b, Å	c, Å	Al_2O_3, %
GD_1	1	43542	$Gd_{2.74}Ce_{0.01}Sc_{0.5}Al_{4.75}O_{12}$	0.01	0.5	1.0381	0.5613	0.39	0.3757	0.9166	100	12.12865(5)	–	–	–	–	–
GD_2	2	54744	$Gd_{2.73}Ce_{0.02}Sc_{0.5}Al_{4.75}O_{12}$	0.02	0.5	1.0384	0.5613	0.39	0.3756	0.9163	100	12.13044(7)	–	–	–	–	–
GD_3	3	39719	$Gd_{2.71}Ce_{0.04}Sc_{0.5}Al_{4.75}O_{12}$	0.04	0.5	1.0390	0.5613	0.39	0.3754	0.9158	100	12.12544(6)	–	–	–	–	–
GD_4	4	-	$Gd_{2.67}Ce_{0.08}Sc_{0.5}Al_{4.75}O_{12}$	0.08	0.5	1.0402	0.5613	0.39	0.3749	0.9148	97.2	12.12796(4)	2.8	5.276(3)	5.291(8)	7.482(4)	–
GD_5	5	-	$Gd_{2.59}Ce_{0.16}Sc_{0.5}Al_{4.75}O_{12}$	0.16	0.5	1.0426	0.5613	0.39	0.3741	0.9128	86.2	12.12883(6)	13.8	5.2939(6)	5.2883(5)	7.4746(6)	–
GD_6	6	13460	$Gd_{2.74}Ce_{0.01}Sc_{1.0}Al_{4.25}O_{12}$	0.01	1.0	1.0381	0.6138	0.39	0.3757	0.9942	100	12.20752(4)	–	–	–	–	–
GD_7	7	12260	$Gd_{2.73}Ce_{0.02}Sc_{1.0}Al_{4.25}O_{12}$	0.02	1.0	1.0384	0.6138	0.39	0.3756	0.9940	100	12.19473(8)	–	–	–	–	–
GD_8	8	21464	$Gd_{2.71}Ce_{0.04}Sc_{1.0}Al_{4.25}O_{12}$	0.04	1.0	1.0390	0.6138	0.39	0.3754	0.9935	100	12.20626(5)	–	–	–	–	–
GD_9	9	5432	$Gd_{2.67}Ce_{0.08}Sc_{1.0}Al_{4.25}O_{12}$	0.08	1.0	1.0402	0.6138	0.39	0.3749	0.9926	100	12.20592(5)	–	–	–	–	–
GD_{10}	10	-	$Gd_{2.59}Ce_{0.16}Sc_{1.0}Al_{4.25}O_{12}$	0.16	1.0	1.0426	0.6138	0.39	0.3741	0.9907	96.7	12.20627(6)	3.3	5.289(5)	5.290(5)	7.491(2)	–
GD_{11}	11	29895	$Gd_{2.74}Ce_{0.01}Sc_{2.0}Al_{3.25}O_{12}$	0.01	2.0	1.0381	0.7188	0.39	0.3757	1.1389	100	12.36616(5)	–	–	–	–	–
GD_{12}	12	35226	$Gd_{2.73}Ce_{0.02}Sc_{2.0}Al_{3.25}O_{12}$	0.02	2.0	1.0384	0.7188	0.39	0.3756	1.1387	100	12.36870(7)	–	–	–	–	–
GD_{13}	13	26055	$Gd_{2.71}Ce_{0.04}Sc_{2.0}Al_{3.25}O_{12}$	0.04	2.0	1.0390	0.7188	0.39	0.3754	1.1383	100	12.37142(4)	–	–	–	–	–
GD_{14}	14	14675	$Gd_{2.67}Ce_{0.08}Sc_{2.0}Al_{3.25}O_{12}$	0.08	2.0	1.0402	0.7188	0.39	0.3749	1.1375	100	12.37275(4)	–	–	–	–	–
GD_{15}	15	620	$Gd_{2.59}Ce_{0.16}Sc_{2.0}Al_{3.25}O_{12}$	0.16	0.5	1.0426	0.7188	0.39	0.3741	1.1359	100	12.37959(8)	–	–	–	–	–
GD_{16}	16	-	$Gd_{2.89}Ce_{0.01}Sc_{0.5}Al_{4.6}O_{12}$	0.01	0.5	1.0472	0.5770	0.39	0.3724	0.9328	90.9	12.15020(6)	9.1	5.3008(3)	5.2556(3)	7.4508(3)	–
GD_{17}	17	-	$Gd_{2.88}Ce_{0.02}Sc_{0.5}Al_{4.6}O_{12}$	0.02	0.5	1.0475	0.5770	0.39	0.3723	0.9325	90.5	12.14947(5)	9.5	5.3001(3)	5.2575(2)	7.4518(3)	–
GD_{18}	18	-	$Gd_{2.86}Ce_{0.04}Sc_{0.5}Al_{4.6}O_{12}$	0.04	0.5	1.0481	0.5770	0.39	0.3721	0.9320	88.9	12.14634(5)	11.1	5.2988(3)	5.2608(2)	7.4553(3)	–
GD_{19}	19	-	$Gd_{2.82}Ce_{0.08}Sc_{0.5}Al_{4.6}O_{12}$	0.08	0.5	1.0493	0.5770	0.39	0.3717	0.9310	86.2	12.14048(5)	13.8	5.2980(3)	5.2676(2)	7.4601(3)	–
GD_{20}	20	-	$Gd_{2.74}Ce_{0.16}Sc_{0.5}Al_{4.6}O_{12}$	0.16	1.0	1.0517	0.5770	0.39	0.3708	0.9290	81.1	12.13351(6)	18.9	5.2971(3)	5.2805(3)	7.4716(4)	–
GD_{21}	21	24136	$Gd_{2.78}Ce_{0.02}Sc_{1.0}Al_{4.2}O_{12}$	0.02	1.0	1.0414	0.6190	0.39	0.3745	0.9992	100	12.22734(7)	–	–	–	–	–
GD_{22}	22	17123	$Gd_{2.58}Ce_{0.02}Sc_{1.0}Al_{4.4}O_{12}$	0.02	1.0	1.0292	0.5980	0.39	0.3789	0.9784	100	12.17052(8)	–	–	–	–	–
GD_{23}	23	10966	$Gd_{2.38}Ce_{0.02}Sc_{1.0}Al_{4.6}O_{12}$	0.02	1.0	1.0170	0.5770	0.39	0.3835	0.9574	100	12.11081(7)	–	–	–	–	–
GD_{24}	24	8369	$Gd_{2.18}Ce_{0.02}Sc_{1.0}Al_{4.8}O_{12}$	0.02	1.0	1.0048	0.5560	0.39	0.3881	0.9362	93.1	12.09974(6)	–	–	–	–	6.9
GD_{25}	25	-	$Gd_{2.98}Ce_{0.02}Al_{5.0}O_{12}$	0.02	–	1.0536	0.5350	0.39	0.3702	0.8622	27.0	12.1124(2)	63.5	–	–	–	9.5

This effect may be explained by the underlying requirement to maintain a certain ratio between the cations' radii located in different garnet sites. Compositions with a total scandium concentration of 1.0 f.u. and a cerium concentration of 0.02 f.u. (GD_{21} – GD_{24}) remained stable until the introduction of 0.6 f.u. Sc to the dodecahedral garnet site. When an attempt was made to synthesize a sample of the $Gd_{2.18}Ce_{0.02}Sc_{1.0}Al_{4.8}O_{12}$ composition after annealing at 1600 °C, the aluminum oxide impurity phase was found in the diffraction patterns (Fig. 2). For comparison, see diffractogram of the GD_{25} sample ($Gd_{2.98}Ce_{0.02}Al_{5.0}O_{12}$), synthesized without scandium in Fig. 2. After annealing at 1600 °C, the mechanical mixture included only 27 wt.%. of garnet phase, 63.5 wt.% of $GdAlO_3$ and 9.5 wt.% of Al_2O_3 (Table 1). These results show that there is a certain range of GSAG:Ce solid solution compositions, in which scandium exhibits the property of impurities that stabilize the garnet phase.

We note that attempts to experimentally determine the compositions that are stable under the powders' synthesis conditions, the ceramics' fabrication, or the growth of single crystals have been repeatedly undertaken for certain types of garnets [20–24]. Empirical equations have been successfully developed to estimate the calculated values of the unit cell parameters for both existing and not yet synthesized garnets [29,30]. In addition, there were few attempts to develop mathematical methods to describe structural relationships describing oxide compositions that form stable phases of garnet [31,32].

Song et al. [30] proposed the use of tolerance factor to measure the garnets' stability, which also binds the effective ionic radii of cations in different sites and anions. In the case of oxide garnets, the tolerance factor range within which the compositions remain stable was determined as 0.748 - 1.333 [30]. All compositions considered in this study met this requirement (Table 1), and should have remained stable which is not the case. This indicates that currently there are no reliable theories and models that could be applied to predict the compositions of stable scandium-containing solid solutions.

SEM and EDX studies were used to obtain additional information about the morphology and phase composition of the synthesized samples. Fig. 3 shows SEM micrographs of powders GD_1 – GD_{15} after annealing at 1600 °C. All studied samples had a similar morphology and consisted of densely sintered aggregates. At the same time, for GD_1 => GD_5, GD_6 => GD_{10}, and GD_{11} => GD_{15} series, an increase in particle size was observed with increase in scandium concentration. It should also be noted that the presence of an impurity phase was found in the GD_5 sample when studying the surface in the backscattered electrons mode (BSE), which correlates well with the X-ray phase analysis data. The absence of impurity phases according to SEM data in GD_4 and GD_{10} samples can be attributed to their presence in miniscule quantities (3 wt%, Table 1).

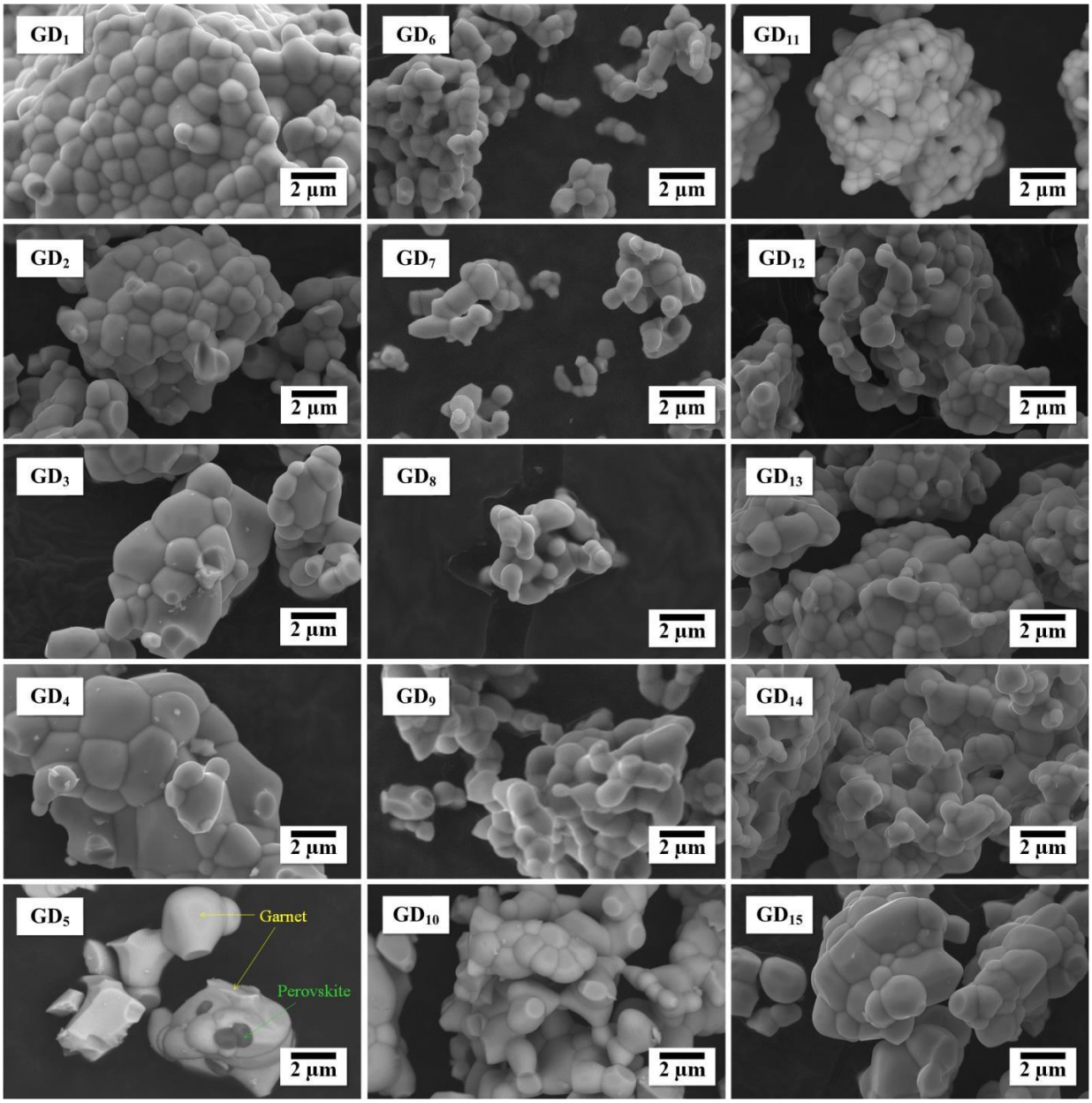

Figure 3. SEM micrographs of ceramic powders of composition GD1 - GD15

The morphology of powders GD_{21} – GD_{25} are presented in Fig. 4. The shape and size of the particles were comparable to those in the samples GD_1 – GD_{15} despite the differences in the synthesis method. At the same time, an increase in the scandium content in the dodecahedral garnet site (GD_{21}=>GD_{24}) led to an increase in the crystallite size and a decrease in the density of aggregates. Of all the samples, GD_{25} composition should be considered separately, since this material contained three phases (garnet, perovskite, aluminum oxide). Its structure was inhomogeneous, characterized by a tendency to strong agglomeration on the one hand and relative fragility on the other, which is evidenced by the presence of aggregate fragments with a smooth surface at the cleavage site.

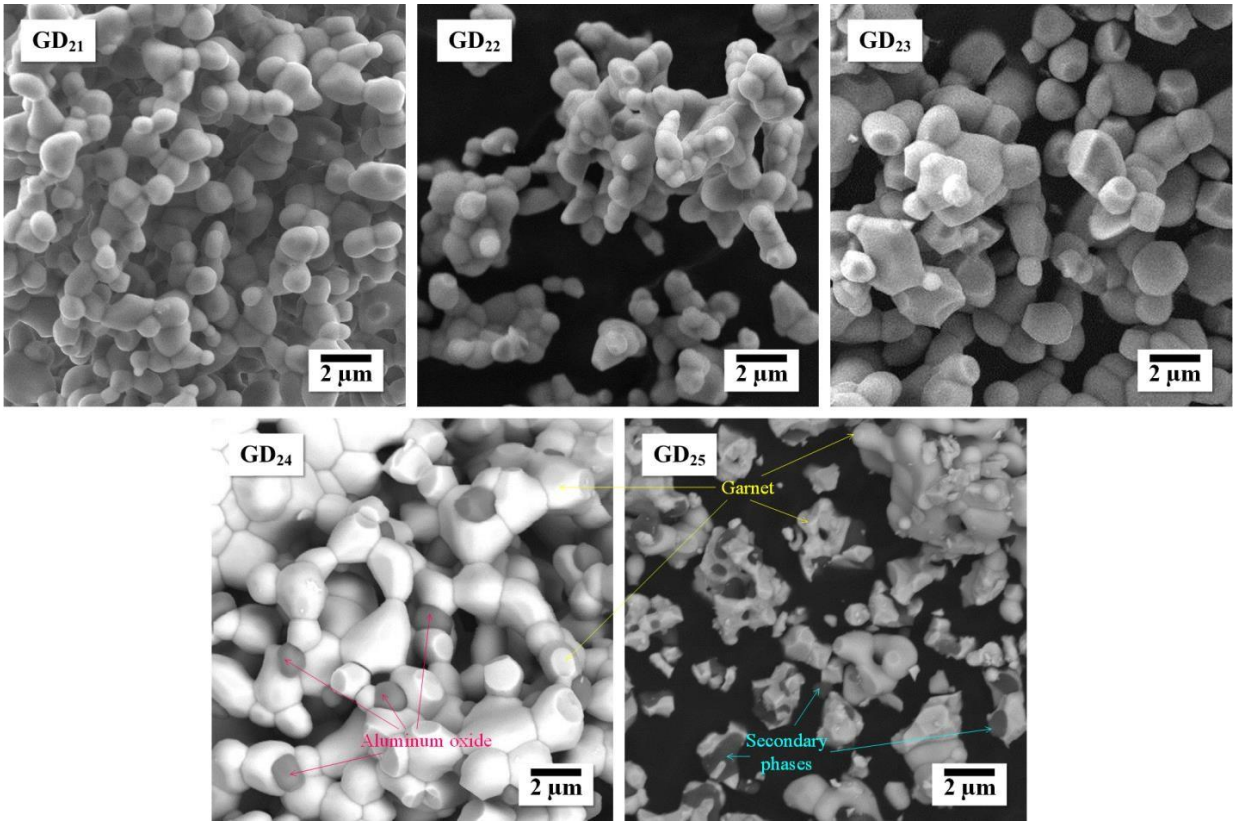

Figure 4. SEM micrographs of ceramic powders of GD_{21} – GD_{25} composition

For all the obtained single-phase solid solutions, their XRL spectra were recorded and are shown in Fig. 5. The main feature for all the samples was an intense peak at ~575 nm, which is attributed to 5d→4f transition in Ce^{3+} ions [6,7]. The XRL intensities for different compositions are summarized in Table 1. In the set of GD_1-GD_3 samples, the XRL intensity is maximized in GD_2 composition (Fig.5a). In GD_6-GD_9 sample series, a similar trend with a maximized XRL in GD_8 sample was observed with a concentration of cerium and scandium being two times higher than for the GD_2 sample (Fig.5b). In GD_{11}-GD_{15} series, the GD_{12} composition with the same Ce content as for GD_2 showed the locally highest XRL intensity (Fig. 5c). Finally, the GD_{21} sample was the one with the highest XRL intensity in GD_{21}-GD_{24} sample series (Fig. 5d). The common trend for GD_2, GD_8, GD_{12}, and GD_{21} samples were the fact that the increase in scandium content results in decreasing XRL intensity. This phenomenon was in accordance with the results seen previously [6] for the garnets, yttrium-aluminum and yttrium-scandium-aluminum, doped with cerium. The highest intensity of XRL among all the studied compositions was registered for $Gd_{2.73}Ce_{0.02}Sc_{0.5}Al_{4.75}O_{12}$ composition (GD_2). In the work by Kling et al.[10], similar luminescence spectra of cerium at various types of exciting radiation were registered for the single crystal $Gd_{2.97}Ce_{0.03}Sc_2Al_3O_{12}$. The difference in the composition determined in our work and presented in the literature lies in the fact that our work reliably determined the distribution of scandium over the dodecahedral and octahedral positions of garnet and the cerium content. The composition of powders synthesized by precipitation from aqueous solutions does not change over the entire volume of the sample, while compositions of single crystals that were grown by the Czochralski method were not properly determined and may vary in the melt due to deviations in the distribution coefficient of cerium between the melt and the crystal.

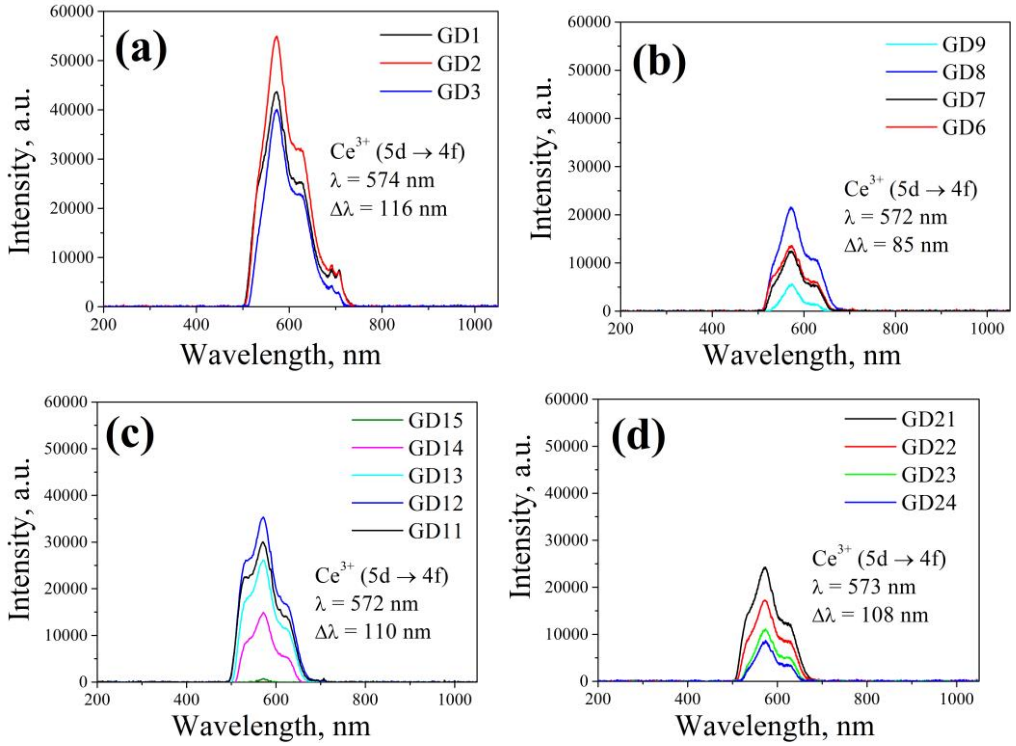

Fig. 5. X-ray luminescence spectra of single-phase solid solutions powders of cerium-doped gadolinium-scandium-aluminum garnets: (a) GD_1-GD_3, (b) GD_6-GD_9, (c) GD_{11}-GD_{15}, (d) GD_{21}-GD_{24}.

The obtained "Diamond-GSAG:Ce" composite consisted of the polycrystalline diamond matrix with integrated particles of the selected GD_2 composition. SEM images showed no defects and residual particles on the surface of diamond films (Fig 6a). However, in cross-sectional micrographs of the obtained composite films, particles with sizes of ~1 μm were observed both in "secondary electrons" (SE) (Fig. 6b) and "backscattered electrons" (BSE) (Fig. 6c) modes of the microscope. The BSE mode has an exceptionally high contrast between lighter carbon and heavier Al/Ce/Gd/Sc atoms (see e.g. [33]). PL spectrum of the obtained composite showed extremely bright but only a local signal from GSAG:Ce particles, the intensity of which was higher than the intensity for the brightest PL peak of the regular diamond film (silicon-vacancy peak, Si-V, 738 nm [34,35]) by 3 orders of magnitude (Fig. 6d) The XRL spectrum of the "Diamond-GSAG:Ce" composite also showed an intense Ce^{3+}-related maximum near 575 nm (Fig. 6e). The intensity of the registered XRL in composite was expectedly lower than for pure GD_2 powder, although the peak position and full width at half maximum were comparable with ones shown in Fig. 5a.

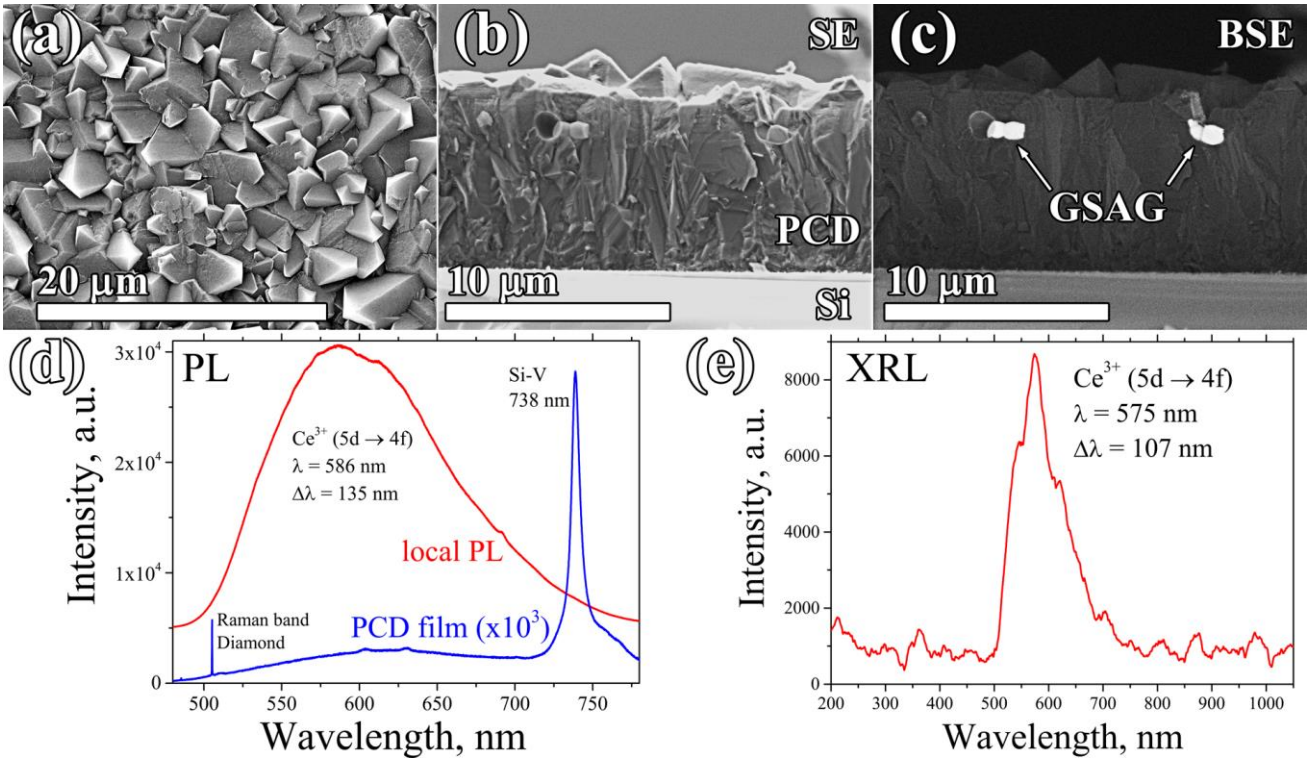

Fig. 6. SEM images of the "Diamond-GSAG:Ce" (GD_2) composite film: (a) surface, (b) cross-section, SE mode, (c) cross-section, BSE mode. (d) PL and (e) XRL spectra of the "Diamond-GSAG:Ce" composite.

To test the obtained "Diamond-GSAG:Ce" material as a source of visible XRL, a set of 4 membranes (5 mm in diameter each, Fig. 7a) with different amount of integrated GD_2 particles (1÷4 drops) was prepared using the method described elsewhere [36]. The XRL properties of the obtained membranes were investigated using "open-chamber" setup that allowed taking photos of samples under X-ray radiation (Fig. 7b). All the membranes showed intense yellow luminescence that is clearly visible both on photographs and to the eye. The addition of the 2nd drop of GD_2 particles after the 1st one led to an increase of the overall XRL intensity of the composite however decreased the homogeneity of its distribution (note in Fig. 7b). The addition of 3rd and 4th drops resulted in increasing inhomogeneity and even led to the formation of macroscopic defects in diamond films.

The XRL spectra (Fig. 7c) showed the similarity of the obtained signal from membranes with spectrum of the "Diamond-GSAG:Ce" film (Fig. 6e). The only difference between spectra taken in 2 different setups was the presence of notable Si-V signal (738 nm) (Fig. 7(c)), which is usually negligibly weak under X-ray excitation in Si-doped diamond films [5,37]. However, we observed similar effect in our previous work on "Diamond-YAG:Ce" composites under high-intensity X-ray radiation and attributed this effect to the excitation of Si-V luminescence by photoelectrons ejected from YAG:Ce nanoparticles [7]. Also note in Fig. 7c that the intensity of Si-V peak correlates with the intensity of Ce^{3+} peak, which is in good agreement with our explanation.

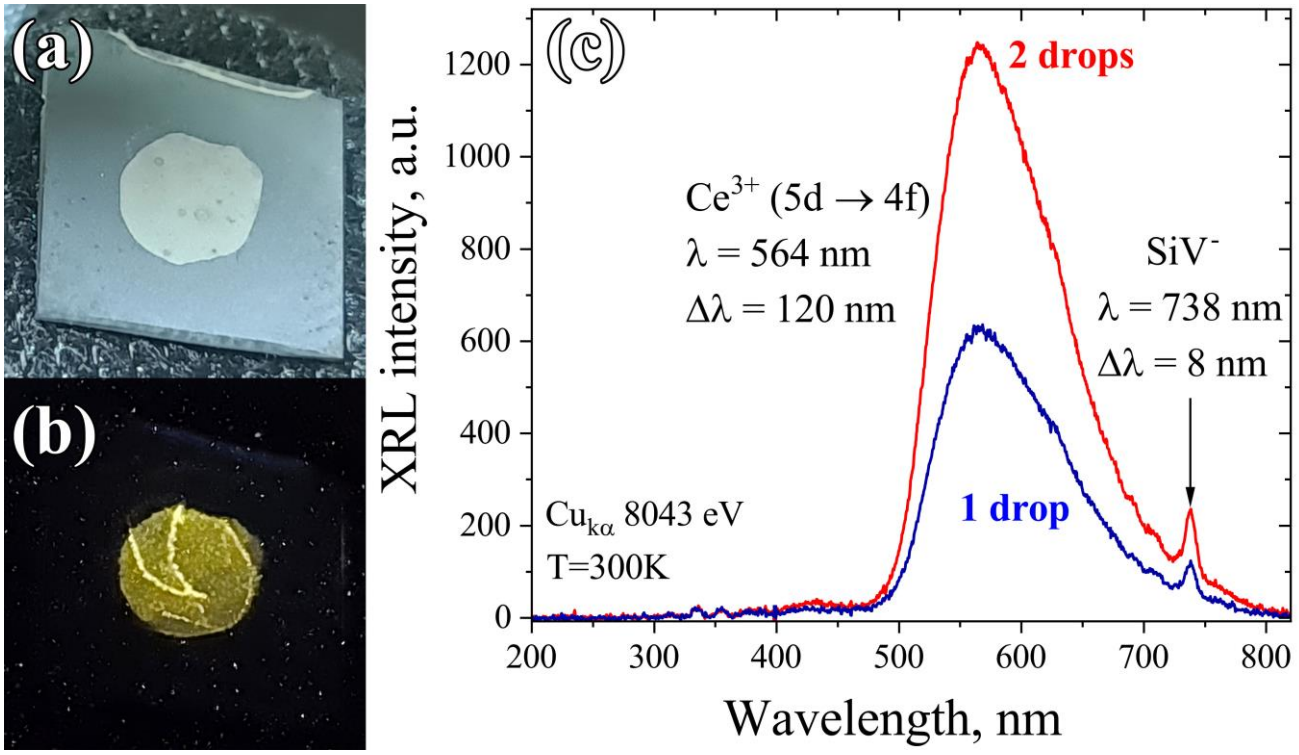

Fig. 7. Photographs of "Diamond-GSAG:Ce" membranes prepared with 2 drops of GD_2 powder in and under X-ray radiation (b), as well as . Note in (b) white speckles as artifacts caused by exposure to X-ray radiation. The inhomogeneity of luminescence in (b) is due to inhomogeneity of distribution of GSAG:Ce particles in composite.

Conclusion

The stable compositions for single-phase solid solutions based on cerium-doped gadolinium-scandium-aluminum garnets are determined. A detailed examination of the studied compositions revealed that, for scandium-containing compositions, there is a tendency towards a regular expansion of the number of available compositions in terms of the r^{IV}/r^{VIII} ratio as the radius of the octahedral garnet site increases. When r^{IV} = const in the compositions under consideration, there is a possibility for obtaining stable garnets with a large ionic radius of the dodecahedral site. At thesame time, the possibility of stabilizing gadolinium-aluminum garnet by replacing the dodecahedral garnet site with scandium was experimentally confirmed. Based on the set of X-ray luminescence spectra of single-phase samples, the composition ($Gd_{2.73}Ce_{0.02}Sc_{0.5}Al_{4.75}O_{12}$), which demonstrates the highest X-ray luminescence, was determined. Finally, the optimized composition was used to synthesize a diamond-based X-ray luminescent films and membranes that showed visible yellow luminescence under X-ray excitation. The investigated class of composites is promising for applications in stable detectors and visualizers of high-intensity X-ray radiation in synchrotrons and free-electron lasers.

Acknowledgments

The reported study was funded by RFBR, project N◦20-32-70074. The studies were carried out using the equipment of the Shared Use Center of North-Caucasus Federal University.

References

1. Magyar, A.; Hu, W.; Shanley, T.; Flatté, M.E.; Hu, E.; Aharonovich, I. Synthesis of Luminescent Europium Defects in Diamond. *Nature communications* **2014**, *5*, 1–6.
2. Sedov, V.S.; Kuznetsov, S.V.; Ralchenko, V.G.; Mayakova, M.N.; Krivobok, V.S.; Savin, S.S.; Zhuravlev, K.P.; Martyanov, A.K.; Romanishkin, I.D.; Khomich, A.A. Diamond-EuF3 Nanocomposites with Bright Orange Photoluminescence. *Diamond and Related Materials* **2017**, *72*, 47–52.

3. Chen, J.-X.; Wang, X.-P.; Wang, L.-J.; Yang, X.-W.; Yang, Y. White Electroluminescence of Diamond/HoF3/Diamond Composite Film. *Journal of Luminescence* **2020**, *224*, 117310.
4. Chen, H.-J.; Wang, X.-P.; Wang, L.-J.; Ke, X.-L.; Ning, R.-M.; Song, M.-L.; Liu, L.-H. Bright Blue Electroluminescence of Diamond/CeF3 Composite Films. *Carbon* **2016**, *109*, 192–195.
5. Sedov, V.; Kouznetsov, S.; Martyanov, A.; Proydakova, V.; Ralchenko, V.; Khomich, A.; Voronov, V.; Batygov, S.; Kamenskikh, I.; Spassky, D.; et al. Diamond–Rare Earth Composites with Embedded $NaGdF_4$:Eu Nanoparticles as Robust Photo- and X-Ray-Luminescent Materials for Radiation Monitoring Screens. *ACS Appl*. *Nano Mater*. **2020**, *3*, 1324–1331.
6. Kuznetsov, S.V.; Sedov, V.S.; Martyanov, A.K.; Batygov, S.Ch.; Vakalov, D.S.; Savin, S.S.; Tarala, V.A. X-Ray Luminescence of Diamond Composite Films Containing Yttrium-Aluminum Garnet Nanoparticles with Varied Composition of Sc–Ce Doping. *Ceramics International* **2021**, *47*, 13922–13926, doi:10.1016/j.ceramint.2021.01.259.
7. Sedov, V.; Kuznetsov, S.; Kamenskikh, I.; Martyanov, A.; Vakalov, D.; Savin, S.; Rubtsova, E.; Tarala, V.; Omelkov, S.; Kotlov, A.; et al. Diamond Composite with Embedded YAG:Ce Nanoparticles as a Source of Fast X-Ray Luminescence in the Visible and near-IR Range. *Carbon* **2021**, *174*, 52–58, doi:10.1016/j.carbon.2020.12.020.
8. Pikuz, T.; Faenov, A.; Matsuoka, T.; Matsuyama, S.; Yamauchi, K.; Ozaki, N.; Albertazzi, B.; Inubushi, Y.; Yabashi, M.; Tono, K. 3D Visualization of XFEL Beam Focusing Properties Using LiF Crystal X-Ray Detector. *Scientific Reports* **2015**, *5*, 17713.
9. Devys, L.; Dantelle, G.; Laurita, G.; Homeyer, E.; Gautier-Luneau, I.; Dujardin, C.; Seshadri, R.; Gacoin, T. A Strategy to Increase Phosphor Brightness: Application with Ce^{3+}-Doped $Gd_3Sc_2Al_3O_{12}$. *Journal of Luminescence* **2017**, *190*, 62–68.
10. Kling, A.; Kollewe, D.; Mateika, D. Scintillation Properties of Cerium-Doped Gadolinium-Scandium-Aluminum Garnets. *Nuclear Instruments and Methods in Physics Research Section A: Accelerators, Spectrometers, Detectors and Associated Equipment* **1994**, *346*, 205–212.
11. Liu, G.; Wang, B.; Li, J.; Cao, B.; Lu, Y.; Liu, Z. Research Progress of Gadolinium Aluminum Garnet Based Optical Materials. *Physica B: Condensed Matter* **2021**, *603*, 412775.
12. Kozlova, A.P.; Kasimova, V.M.; Buzanov, O.A.; Chernenko, K.; Klementiev, K.; Pankratov, V. Luminescence and Vacuum Ultraviolet Excitation Spectroscopy of Cerium Doped Gd3Ga3Al2O12 Single Crystalline Scintillators under Synchrotron Radiation Excitations. *Results in Physics* **2020**, *16*, 103002.
13. Li, J.; Li, J.-G.; Zhang, Z.; Wu, X.; Liu, S.; Li, X.; Sun, X.; Sakka, Y. Gadolinium Aluminate Garnet (Gd3Al5O12): Crystal Structure Stabilization via Lutetium Doping and Properties of the (Gd 1- x Lu x) 3 Al5O12 Solid Solutions (X= 0–0.5). *Journal of the American Ceramic Society* **2012**, *95*, 931–936.
14. Li, J.-G.; Sakka, Y. Recent Progress in Advanced Optical Materials Based on Gadolinium Aluminate Garnet (Gd3Al5O12). *Science and technology of advanced materials* **2015**.
15. Mahlik, S.; Kuklinski, B.; Grinberg, M.; Kostyk, L.; Tsvetkova, O. Luminescence and Luminescence Kinetics of Gd3Ga5O12 Polycrystals Doped with Cr3+ and Pr3+. *Acta Physica Polonica-Series A General Physics* **2010**, *117*, 117.
16. Shannon, R.D. Revised Effective Ionic Radii and Systematic Studies of Interatomic Distances in Halides and Chalcogenides. *Acta crystallographica section A: crystal physics, diffraction, theoretical and general crystallography* **1976**, *32*, 751–767.
17. Li, J.K.; Li, J.G.; Wu, X.L.; Liu, S.H.; Li, X.D.; Sun, X.D. Crystal Structure Stabilization of Gadolinium Aluminum Garnet (Gd3Al5O12) and Photoluminescence Properties. In Proceedings of the Key Engineering Materials; Trans Tech Publ, 2013; Vol. 544, pp. 245–251.
18. Li, J.; Li, J.-G.; Li, X.; Sun, X. Up-Conversion Luminescence of New Phosphors of Gd3Al5O12: Yb/Er Stabilized with Lu3+. *Ceramics International* **2016**, *42*, 3268–3274.
19. Li, J.; Li, J.-G.; Liu, S.; Li, X.; Sun, X.; Sakka, Y. The Development of Ce3+-Activated (Gd, Lu) 3Al5O12 Garnet Solid Solutions as Efficient Yellow-Emitting Phosphors. *Science and technology of advanced materials* **2013**.
20. Nikova, M.S.; Tarala, V.A.; Vakalov, D.S.; Kuleshov, D.S.; Kravtsov, A.A.; Kuznetsov, S.V.; Chikulina, I.S.; Malyavin, F.F.; Tarala, L.V.; Evtushenko, E.A. Temperature-Related Changes in the Structure of YSAG: Yb Garnet Solid Solutions with High Sc3+ Concentration. *Journal of the European Ceramic Society* **2019**, *39*, 4946–4956.
21. Tarala, V.A.; Shama, M.S.; Chikulina, I.S.; Kuznetsov, S.V.; Malyavin, F.F.; Vakalov, D.S.; Kravtsov, A.A.; Pankov, M.A. Estimation of Sc3+ Solubility in Dodecahedral and Octahedral Sites in YSAG: Yb. *Journal of the American Ceramic Society* **2019**, *102*, 4862–4873.
22. Nikova, M.S.; Tarala, V.A.; Malyavin, F.F.; Vakalov, D.S.; Lapin, V.A.; Kuleshov, D.S.; Kravtsov, A.A.; Chikulina, I.S.; Tarala, L.V.; Evtushenko, E.A. The Scandium Impact on the Sintering of YSAG: Yb Ceramics with High Optical Transmittance. *Ceramics International* **2021**, *47*, 1772–1784.
23. Petrosyan, A.G.; Ovanesyan, K.L.; Shirinyan, G.O.; Sargsyan, R.V.; Dujardin, C.; Pedrini, C. Site Occupation and Solubility Limit of Sc in Lu3Al5O12. *Journal of crystal growth* **2012**, *338*, 143–146.

24. Lutts, G.B.; Denisov, A.L.; Zharikov, E.V.; Zagumennyi, A.I.; Kozlikin, S.N.; Lavrishchev, S.V.; Samoylova, S.A. GSAG and YSAG: A Study on Isomorphism and Crystal Growth. *Optical and quantum electronics* **1990**, *22*, S269–S281.
25. Kaurova, I.A.; Domoroshchina, E.N.; Kuz'micheva, G.M.; Rybakov, V.B. Evaluation of Stability Region for Scandium-Containing Rare-Earth Garnet Single Crystals and Their Congruent-Melting Compositions. *Journal of Crystal Growth* **2017**, *468*, 452–456.
26. Sedov, V.; Martyanov, A.; Khomich, A.; Savin, S.; Zavedeev, E.; Ralchenko, V. Deposition of Diamond Films on Si by Microwave Plasma CVD in Varied CH_4-H_2 Mixtures: Reverse Nanocrystalline-to-Microcrystalline Structure Transition at Very High Methane Concentrations. *Diamond and Related Materials* **2020**, *109*, 108072.
27. Hees, J.; Kriele, A.; Williams, O.A. Electrostatic Self-Assembly of Diamond Nanoparticles. *Chemical Physics Letters* **2011**, *509*, 12–15, doi:10.1016/j.cplett.2011.04.083.
28. Mandal, S. Nucleation of Diamond Films on Heterogeneous Substrates: A Review. *RSC Advances* **2021**, *11*, 10159–10182.
29. Vorobiov, Y.P.; Carban, O.V. A New Empirical Formula for the Calculation of an Elementary Cell Parameter of Synthetic Oxides–Garnets. *Journal of Solid State Chemistry* **1997**, *134*, 338–343.
30. Strocka, B.; Holst, P.; Tolksdorf, W. An Empirical Formula for the Calculation of Lattice Constants of Oxide Garnets Based on Substituted Yttrium-and Gadolinium-Iron Garnets. *Philips Journal of Research* **1978**, *33*, 186–202.
31. Song, Z.; Zhou, D.; Liu, Q. Tolerance Factor and Phase Stability of the Garnet Structure. *Acta Crystallographica Section C: Structural Chemistry* **2019**, *75*, 1353–1358.
32. Vorobiev, Y. Defects of Laser Crystals and Magnetic Ceramics. *Ural Branch of the Russian Academy of Sciences, Yekaterinburg* **2006**.
33. Sedov, V.S.; Martyanov, A.K.; Khomich, A.A.; Savin, S.S.; Voronov, V.V.; Khmelnitskiy, R.A.; Bolshakov, A.P.; Ralchenko, V.G. Co-Deposition of Diamond and β-SiC by Microwave Plasma CVD in H2-CH4-SiH4 Gas Mixtures. *Diamond and Related Materials* **2019**, *98*, 107520.
34. Sedov, V.; Ralchenko, V.; Khomich, A.A.; Vlasov, I.; Vul, A.; Savin, S.; Goryachev, A.; Konov, V. Si-Doped Nano- and Microcrystalline Diamond Films with Controlled Bright Photoluminescence of Silicon-Vacancy Color Centers. *Diamond and Related Materials* **2015**, *56*, 23–28, doi:10.1016/j.diamond.2015.04.003.
35. Ralchenko, V.G.; Sedov, V.S.; Martyanov, A.K.; Bolshakov, A.P.; Boldyrev, K.N.; Krivobok, V.S.; Nikolaev, S.N.; Bolshedvorskii, S.V.; Rubinas, O.R.; Akimov, A.V.; et al. Monoisotopic Ensembles of Silicon-Vacancy Color Centers with Narrow-Line Luminescence in Homoepitaxial Diamond Layers Grown in H2–CH4–[x]SiH4 Gas Mixtures (x = 28, 29, 30). *ACS Photonics* **2019**, *6*, 66–72, doi:10.1021/acsphotonics.8b01464.
36. Sedov, V.S.; Voronin, A.A.; Komlenok, M.S.; Savin, S.S.; Martyanov, A.K.; Popovich, A.F.; Altakhov, A.S.; Kurochka, A.S.; Markus, D.V.; Ralchenko, V.G. Laser-Assisted Formation of High-Quality Polycrystalline Diamond Membranes. *J Russ Laser Res* **2020**, *41*, 321–326, doi:10.1007/s10946-020-09881-x.
37. Osadchy, A.V.; Vlasov, I.I.; Kudryavtsev, O.S.; Sedov, V.S.; Ralchenko, V.G.; Batygov, S.H.; Savin, V.V.; Ershov, P.A.; Chaika, V.A.; Narikovich, A.S.; et al. Luminescent Diamond Window of the Sandwich Type for X-Ray Visualization. *Appl. Phys. A* **2018**, *124*, 807, doi:10.1007/s00339-018-2230-0.